Designing a minimal Landau model to stabilize desired quasicrystals

Wei Si [1,*] Shifeng Li,[1,3,*] Pingwen Zhang,[2,3,†] An-Chang Shi [4,‡] and Kai Jiang [1,§]
[1]School of Mathematics and Computational Science, Hunan Key Laboratory for Computation and Simulation in Science and Engineering, Xiangtan University, Hunan 411105, China
[2]LMAM, CAPT and School of Mathematical Sciences, Peking University, Beijing 100871, China
[3]School of Mathematics and Statistics, Wuhan University, Wuhan 430072, China
[4]Department of Physics and Astronomy, McMaster University, Hamilton L8S 4M1, Canada

(Received 13 January 2025; accepted 11 March 2025; published 7 April 2025)

Interparticle interactions with multiple length scales play a pivotal role in the formation and stability of quasicrystals. Choosing a minimal set of length scales to stabilize a given quasicrystal is a challenging problem. To address this challenge, we propose a symmetry-preserving screening method (SPSM) to design a Landau theory with a minimal number of length scales—referred to as the minimal Landau theory—that includes only the essential length scales necessary to stabilize quasicrystals. Based on a generalized multiple-length-scale Landau theory, SPSM first evaluates various spectral configurations of candidate structures under a hard constraint. It then identifies the configuration with the lowest free energy. Using this optimal configuration, SPSM calculates phase diagrams to explore the thermodynamic stability of desired quasicrystals. SPSM can design a minimal Landau theory capable of stabilizing the desired quasicrystals by incrementally increasing the number of length scales. Our application of SPSM has not only confirmed known behaviors in 10- and 12-fold quasicrystals but also led to a significant prediction that quasicrystals with 8-, 14-, 16-, and 18-fold symmetry could be stable within three-length-scale Landau models.

DOI: 10.1103/PhysRevResearch.7.023021

I. INTRODUCTION

Quasicrystals (QCs) are ordered structures that exhibit rotational symmetry but lack translational symmetry. Since the first discovery of QCs in Al-Mn alloys [1], QCs have attracted tremendous attention in material science and condensed matter physics [2–9]. In recent years, QCs have been discovered in a variety of soft condensed matter, including micelle-forming liquid crystals [3,8,10–12], block copolymers [4,7,13–16], colloidal suspensions [17], and binary mixtures of nanoparticles [18,19]. To date, numerous QCs with 8-, 10-, 12-, and 18-fold rotational symmetries have been frequently reported in both metallic alloys [2] and soft matters [3,6–9,13,15,17,19–22]. Much effort has been devoted to studying the properties of QCs, predicting their stability, and developing methods to control their formation [23,24].

Landau theories have been extensively employed to study the formation, stability and phase transition of ordered phases, including periodic crystals and QCs [25–29]. Generally, a Landau free-energy functional consists of a polynomial-type bulk energy and a nonlocal pairwise interaction,

$$\mathcal{F}[\phi(\boldsymbol{r})] = \fint [d_2\phi(\boldsymbol{r})^2 + d_3\phi(\boldsymbol{r})^3 + d_4\phi(\boldsymbol{r})^4 + \ldots]\, d\boldsymbol{r} + \frac{1}{2}\fint\fint \phi(\boldsymbol{r})C(|\boldsymbol{r}-\boldsymbol{r}'|)\phi(\boldsymbol{r}')\, d\boldsymbol{r}d\boldsymbol{r}', \tag{1}$$

where $\phi(\boldsymbol{r})$ is an order parameter describing the particle distribution, $C(r)$ is the pair direct correlation potential [30] that is finite for the distance r between particles [31]. $C(r) > 0$ reflects an attractive interaction between particles, and $C(r) < 0$ indicates a repulsive interaction. $\fint = \lim_{\Omega\to\mathbb{R}^3} \frac{1}{V(\Omega)} \int_\Omega$ and $V(\Omega)$ is the volume of the region Ω. In the case of a periodic phase, the integral is equivalent to an integral over its unit cell. The power series in the first term of Eq. (1) is typically truncated to the fourth order [32–34]. The quadratic term contributes to the growth of instability, while the quartic term establishes a lower bound for the free energy. The cubic term breaks the $\phi \to -\phi$ symmetry.

An understanding of how to stabilize an ordered structure comes from representing the second term of (1) in reciprocal space,

$$\frac{1}{2}\fint \hat{C}(k)|\hat{\phi}(\boldsymbol{k})|^2\, d\boldsymbol{k},\ k = |\boldsymbol{k}|,$$

where $\boldsymbol{k}$ is the reciprocal lattice vector (RLV), $\hat{\phi}(\boldsymbol{k}) = \fint \exp(-i\boldsymbol{k}\cdot\boldsymbol{r})\phi(\boldsymbol{r})\, d\boldsymbol{r}$ is the Fourier transform of $\phi(\boldsymbol{r})$, and $\hat{C}(k)$ is the Fourier transform of $C(r)$. The Fourier coefficients $\hat{\phi}(\boldsymbol{k})$ with wave numbers at the minima of $\hat{C}(k)$ are

*These authors contributed equally to this work.
†Contact author: pzhang@pku.edu.cn
‡Contact author: shi@mcmaster.ca
§Contact author: kaijiang@xtu.edu.cn

energetically favored. Given the N-fold rotational symmetry, the correlation potential can be approximated by a polynomial with roots $d_1, d_2, \ldots$,

$$\hat{C}(k) \approx c\left(k^2 - d_1^2\right)\left(k^2 - d_2^2\right)\cdots, \quad c > 0. \tag{2}$$

When $\hat{C}(k)$ is truncated to second order, i.e., $c(k^2 - d_1^2)$, which has the minima at $k = 0$, the model can be used to simulate the solidification process of binary mixtures, such as phase-field models [35].

More complex phase behaviors related to multiple length scales can be investigated by the correlation potential with multiple roots [32–34,36–38]. For a single length scale, the potential (2) should be truncated to fourth order and rewritten as $c(k^2 - 1)^2$ by scaling k in units of $\sqrt{(d_1^2 + d_2^2)/2}$ and omitting constant terms. This potential discourages RLVs with wave numbers deviating from the length scale 1. The single-length-scale potential has been extensively utilized to explain phase behaviors in periodic systems, such as Landau-Brazovskii model [32] and Swift-Hohenberg model [33]. To achieve two length scales, $\hat{C}(k)$ must be truncated to eighth order and rewritten as $c[(k^2 - q_1^2)(k^2 - q_2^2)]^2$, which features two equal-depth minima at $k = q_1$ and $k = q_2$. This two-length-scale potential was first proposed by Lifshitz and Petrich (LP) to describe quasiperiodic pattern-forming dynamics [34] and to find stable 12-fold QCs by setting $q_2/q_1 = 2\cos(\pi/12)$. Over the years, this two-length-scale type potential has been widely used to study the thermodynamic stability of QCs and found stable 10-, 12-fold QCs and three-dimensional icosahedral QCs [5,36–43,55].

However, many QCs are metastable or unstable in two-length-scale models, such as 8- and 18-fold QCs. This raises the question: Could these QCs be stabilized by introducing more length scales? Lifshitz and Petrich speculated that correlation potentials with three or four length scales could stabilize higher-order symmetric QCs, such as 18- or 24-fold QCs [34]. Savitz *et al.* have demonstrated that this conjecture might be correct and found stable 8- and 18-fold QCs in four-length-scale Landau models [37]. However, increasing the number of length scales introduces greater complexity in interparticle interactions within physical systems and poses a significant challenge for theoretical analysis [3,13,15,44,45]. Therefore, it is crucial to design a Landau theory with the minimal number of length scales, i.e., the minimal Landau model to stabilize desired QCs.

Designing a minimal Landau theory requires a general Landau model with multiple length scales. To incorporate m length scales, we could truncate Eq. (2) to the $4m$th order and adjust parameters to achieve equal-depth minima at $k = q_1, \ldots, q_m$, thereby rewriting the correlation potential in the form,

$$\hat{C}_m(k) = c\left[\prod_{j=1}^{m}\left(k^2 - q_j^2\right)\right]^2, \quad c > 0. \tag{3}$$

This pair potential favors the RLVs with wave numbers close to the length scales $q_1, \ldots, q_m$ but suppresses the other RLVs. Substituting Eq. (3) into Eq. (1) and truncating the polynomial to fourth order lead to a generalized m-length-scale free-energy functional [37,45]

$$\mathcal{F}_m[\phi(\boldsymbol{r})] = \fint\left(-\frac{\epsilon}{2}\phi^2 - \frac{\alpha}{3}\phi^3 + \frac{1}{4}\phi^4\right)d\boldsymbol{r} + \frac{c}{2}\fint\left[\prod_{j=1}^{m}\left(\nabla^2 + q_j^2\right)\phi(\boldsymbol{r})\right]^2 d\boldsymbol{r}, \tag{4}$$

where the parameter ϵ is temperature-related, α measures the intensity of three-body interaction, $c > 0$ is a penalty factor, and $q_1, \ldots, q_m$ are length scales. The function $\phi(\boldsymbol{r})$ satisfies the mean-zero constraint, $\fint\phi(\boldsymbol{r})\,d\boldsymbol{r} = 0$, corresponding to a mass-conserved system.

We organize the rest of this paper as follows. In Sec. II, we propose an symmetry-preserving screening method to design a minimal Landau theory for desired QCs. In Sec. III, we apply this method to design minimal Landau theories for $2n$-fold QCs ($n = 4, 5, \ldots, 9$). We find that three-length-scale Landau models can stabilize 8-, 14-, 16-, and 18-fold QCs. Finally, we summarize this paper in Sec. IV.

II. SYMMETRY-PRESERVING SCREENING METHOD (SPSM)

Designing a minimal Landau theory to stabilize desired QCs requires considering various candidate structures. For a candidate phase, there are numerous possible configurations of RLVs describing its spectral distribution. To identify the optimal configuration with the lowest free energy, it is crucial to analyze the contributions of RLVs.

RLVs could be categorized into primary and nonprimary RLVs. The primary RLVs exhibit strong intensities and have wave numbers equal to the length scales. The remaining RLVs are the nonprimary RLVs. Numerous studies indicate that the primary RLVs determine the main characteristics of ordered structures and the nonprimary RLVs influence local details [36,37,46,55]. The contributions of primary and nonprimary RLVs can be studied from two perspectives: hard constraint (HC) with $c \to \infty$, and soft constraint (SC) with a finite c. Under the HC, $\hat{C}_m(k)$ is zero if the wave number k belongs to the set $\{q_1, \ldots, q_m\}$, and otherwise it is infinite. This implies that all nonprimary RLVs are forbidden under this constraint. The SC relaxes the restriction on wave numbers, permitting the emergence of nonprimary RLVs, which may be favored by a realistic system.

Based on the two constraints, we propose SPSM to design a minimal Landau theory to stabilize the desired QCs, as shown in Fig. 1. Given a target QC and the number of length scales, there might be many configurations of primary RLVs. Let us consider HC first. For a specific configuration, HC only allows a finite number of primary RLVs, thus the free-energy functional can be written as a polynomial function. The polynomial function can be easily minimized by computer-assisted symbolic calculation to obtain the free energy of the configuration. Among all configurations, SPSM selects the optimal one with the lowest free energy by directly comparing the free energies. Using the optimal configuration, we can study the thermodynamic stability of the target QC by constructing phase diagrams under HC. If the target QC is metastable or unstable, we increase the number of length scales to obtain

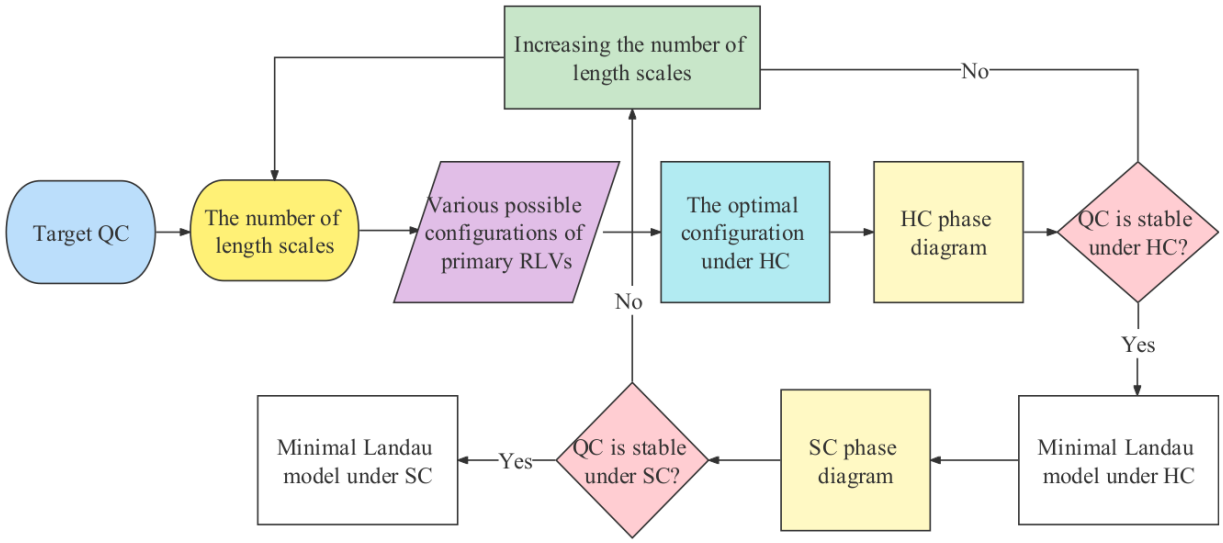

FIG. 1. Flowchart of SPSM. The number of length scales increases gradually from 1.

more configurations. The optimal configuration among these may lead to the formation of a stable QC. The free-energy functional $\mathcal{F}_m$ with these length scales is called a HC minimal Landau model. Based on the optimal configuration and the HC minimal Landau model, we further design a minimal Landau model under SC. Since SC permits the emergence of nonprimary RLVs, we use numerical methods to calculate SC phase diagrams to study the stability of the target QC. We obtain the SC minimal Landau model if the target QC is stable, otherwise, we repeat the above process with more length scales. We can always obtain a minimal Landau theory to stabilize target QC since more length scales have more primary RLVs that may form more triplets to lower the free energy.

In order to obtain the possible configurations of primary RLVs, we first analyze the elements of primary RLVs. For a candidate phase, its primary RLVs are determined by the length scales and the relative positions. As an example, we consider two-length-scale eightfold QCs, as demonstrated in Fig. 2. The length scales are consistent with the radii of the circles q_1 and q_2. The relative positions depend on the offset angles θ_1 and θ_2. The offset angle of each circle is defined as the minimal angle at which the primary RLV rotates clockwise in the horizontal direction. Note that the primary RLVs on each circle are equivalent due to rotational symmetry. Without loss of generality, we set $\theta_1 = 0$ and the rest is $\theta_2 - \theta_1$. For an m-length-scale N-fold candidate phase, we have

$$q_j = \cos(w_j \pi / N), \quad j = 1, \ldots, m, \tag{5}$$

$$\theta_1 = 0, \quad \theta_{j'} = s_{j'} \pi / N, \quad j' = 2, \ldots, m. \tag{6}$$

The primary RLVs given by (5) and (6) can form more triplets, which could lower the free energy. $w_j \in [0, N/2)$ owing to the periodicity of the cosine function, and $s_{j'} \in [0, 2)$ because of rotational symmetry. We obtain various possible configurations of primary RLVs by discretizing w_j and $s_{j'}$ in the valid ranges.

Under HC, the free-energy functional $\mathcal{F}_m$ can be written as a polynomial function. Since $\hat{C}_m(k)$ should be zero to ensure finite free energy, $\mathcal{F}_m$ preserves bulk energy part

$$\mathcal{F}_m = \int \left(-\frac{\epsilon^*}{2}\phi^2 - \frac{1}{3}\phi^3 + \frac{1}{4}\phi^4 \right) d\boldsymbol{r}, \tag{7}$$

where $\epsilon^* = \epsilon/\alpha^2$. Note that Eq. (7) has scaled the cubic coefficient α to unity by measuring the field ϕ in units of α and the energy in units of α^4. Using the Fourier transformation of $\phi(\boldsymbol{r})$, Eq. (7) becomes

$$\begin{aligned} \mathcal{F}_m(\hat{\phi}_{q_1}, \ldots, \hat{\phi}_{q_m}) = & -\frac{\epsilon^*}{2} \sum_{\boldsymbol{k}_1+\boldsymbol{k}_2=\boldsymbol{0}} \hat{\phi}_{k_1}\hat{\phi}_{k_2} \\ & - \frac{1}{3} \sum_{\boldsymbol{k}_1+\boldsymbol{k}_2+\boldsymbol{k}_3=\boldsymbol{0}} \hat{\phi}_{k_1}\hat{\phi}_{k_2}\hat{\phi}_{k_3} \\ & + \frac{1}{4} \sum_{\boldsymbol{k}_1+\boldsymbol{k}_2+\boldsymbol{k}_3+\boldsymbol{k}_4=\boldsymbol{0}} \hat{\phi}_{k_1}\hat{\phi}_{k_2}\hat{\phi}_{k_3}\hat{\phi}_{k_4}, \end{aligned} \tag{8}$$

where all $k_i = |\boldsymbol{k}_i|$ belong to the set $\{q_1, \ldots, q_m\}$, $i = 1, 2, 3, 4$, and $\hat{\phi}_{q_j}$ denotes the Fourier coefficient with wave number q_j. In Eq. (8), the three-RLV interaction in the third

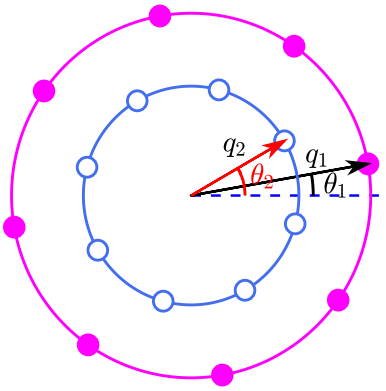

FIG. 2. Primary RLVs of the eightfold QC with two length scales q_1 and q_2. Magenta (royal blue) dots and the origin form the primary RLVs. θ_1 and θ_2 are offset angles.

row is beneficial to lower the free energy, but the four-RLV interaction in the fourth row increases the free energy. Since the primary RLVs are finite for a specific configuration, we can calculate the summations in Eq. (8) by symbolic computation. We then minimize the polynomial function with respective to $\hat{\phi}_{q_1}, \ldots, \hat{\phi}_{q_m}$ to obtain the free energy of this configuration. Among all possible configurations, we select the optimal configuration with the lowest free energy. Using the optimal configuration, we study the thermodynamic stability of desired QCs by constructing a phase diagram under HC.

Under SC, SPSM can also examine the thermodynamic stability of desired QCs by combining with numerical methods. An accurate and efficient numerical approach to study QCs is the projection method [47,48]. The projection method embeds the QC into a high-dimensional periodic system, which can be efficiently calculated by fast Fourier transformation, and then obtains the QC by projecting it back to the original space. The specific formula of the projection method is

$$\phi(\boldsymbol{r}) = \sum_{\boldsymbol{h}\in\mathbb{Z}^{d_1}} \hat{\phi}(\boldsymbol{h}) e^{i(\mathcal{P}\cdot\boldsymbol{h})^T\cdot\boldsymbol{r}}, \quad \boldsymbol{r}\in\mathbb{R}^{d_0}, \quad d_0 \leqslant d_1, \tag{9}$$

where $\mathcal{P}$ is a $d_0 \times d_1$-order projection matrix. d_0 is the dimension of the original space, and d_1 is the dimension of the high-dimensional space dependent on the symmetry of the QC. A special case of $d_0 = d_1$ implies that the projection method is the common Fourier pseudospectral approach for periodic crystals. Moreover, the m-length-scale model under SC can be rescaled to reduce the number of model parameters. Let q_* be any element of the set $\{q_j\}_{j=1}^m$. c is rescaled to unit by measuring the field ϕ in units of $\sqrt{c}q_*^{2m}$, and consequently the energy is measured in units of $c^2 q_*^{8m}$, thus Eq. (4) becomes

$$\mathcal{F}_m[\phi(\boldsymbol{r})] = \fint \left(-\frac{\epsilon}{2}\phi^2 - \frac{\alpha}{3}\phi^3 + \frac{1}{4}\phi^4\right) d\boldsymbol{r} + \frac{1}{2}\fint \left[\prod_{j=1}^{m}\left(\nabla^2 + q_j^2/q_*^2\right)\phi(\boldsymbol{r})\right]^2 d\boldsymbol{r}, \tag{10}$$

where ϵ and α are measured in units of cq_*^{4m} and $\sqrt{c}q_*^{2m}$, respectively. In this paper, q_* takes the minimal value of $\{q_j\}_{j=1}^m$. Its stationary solutions can be quickly and robustly obtained by recently developed optimization methods [49–51]. And its phase diagram can be automatically and efficiently generated by our developed open-source software [52].

III. RESULTS AND DISCUSSIONS

Applying the SPSM, we design minimal Landau theories for two-dimensional $2n$-fold QCs ($n = 4, 5, \ldots, 9$). These QCs are named as octagonal (O), decagonal (D), dodecagonal (DD), tetradecagonal (TD), hexadecagonal (HD), and octadecagonal (OD) QCs, respectively. Note that the primary RLVs with a single length scale could not generate sufficient three-RLV interactions to stabilize QCs in the Landau free-energy functionals [34,46]. We present the numerical results of two, three and four length scales in Supplemental Material (SM) [53]. The results include optimal configurations of primary RLVs, HC free energy, HC phase diagrams, and the SC phase diagrams of minimal Landau models. The results demonstrate that 10- and 12-fold QCs can be stabilized in the Landau model with at least two length scales, which is consistent with previous findings [34,36,40,41,55], implying the effectiveness of SPSM. The results of 8-, 14-, 16- and 18-fold QCs give some exciting predictions, which will be introduced in this section.

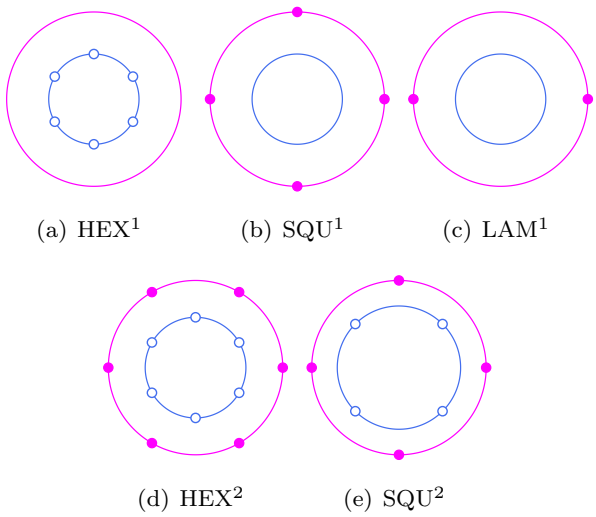

FIG. 3. Optimal primary RLVs of (a)–(c) single-length-scale and (d), (e) two-length-scale competing crystals. Superscripts denote the number of valid length scales. The radius of inner (royal blue) circle is q_1 and the radius of outer (magenta) circle is q_2. q_2/q_1 is equal to (d) $2\cos(\pi/6)$ and (e) $2\cos(\pi/4)$.

In what follows, we consider three competing crystals, including lamellar (LAM), square (SQU), and hexagonal (HEX) crystals to study the thermodynamic stability of an m-length-scale QC. The competing crystals have the length scales consistent with the length scales of the QC. The offset angles follow Eq. (6), where $N = 2$ for LAM, $N = 4$ for SQU, and $N = 6$ for HEX. Under HC, the free-energy functional can be written as a polynomial function, thus we can easily obtain the optimal primary RLVs of these crystals. It should be noted that if the Fourier coefficients at some primary RLVs are very weak or even vanished, i.e., these primary RLVs become nonprimary RLVs, the number of valid length scales of the crystals denoted by superscripts is less than m. Numerical simulations demonstrate the optimal configuration of primary RLVs has one or two valid length scales for HEX and SQU but only one valid length scale for LAM, as shown in Fig. 3. For the case of one valid length scale, the HC free energies are

$$\mathcal{F}_{\mathrm{HEX}^1}(\hat{\phi}_j, \epsilon^*) = -3\epsilon^*\hat{\phi}_j^2 - 4\hat{\phi}_j^3 + \tfrac{45}{2}\hat{\phi}_j^4, \tag{11}$$

$$\mathcal{F}_{\mathrm{SQU}^1}(\hat{\phi}_j, \epsilon^*) = -2\epsilon^*\hat{\phi}_j^2 + 9\hat{\phi}_j^4, \tag{12}$$

$$\mathcal{F}_{\mathrm{LAM}^1}(\hat{\phi}_j, \epsilon^*) = -\epsilon^*\hat{\phi}_j^2 + \tfrac{3}{2}\hat{\phi}_j^4. \tag{13}$$

For the case of two valid length scales, the length scales satisfy a special ratio to form more three-RLV interactions: $q_2/q_1 = 2\cos(\pi/6)$ for HEX^2 and $q_2/q_1 = 2\cos(\pi/4)$ for SQU^2. Their HC free energies are given by

$$\mathcal{F}_{\mathrm{HEX}^2}\left(\{\hat{\phi}_j\}_{j=1}^2, \epsilon^*\right) = -3\epsilon^*\left(\hat{\phi}_1^2 + \hat{\phi}_2^2\right) - 12\hat{\phi}_1^2\hat{\phi}_2$$

$$-4\hat{\phi}_1^3-4\hat{\phi}_2^3+\tfrac{45}{2}\left(\hat{\phi}_1^4+\hat{\phi}_2^4\right)+36\hat{\phi}_1^3\hat{\phi}_2+90\hat{\phi}_1^2\hat{\phi}_2^2, \tag{14}$$

$$\mathcal{F}_{\mathrm{SQU}^2}\left(\{\hat{\phi}_j\}_{j=1}^2,\epsilon^*\right)=-2\epsilon^*\left(\hat{\phi}_1^2+\hat{\phi}_2^2\right)-8\hat{\phi}_1^2\hat{\phi}_2 +9\left(\hat{\phi}_1^4+4\hat{\phi}_1^2\hat{\phi}_2^2+\hat{\phi}_2^4\right). \tag{15}$$

A. Octagonal (O) QCs

Two-dimensional OQCs have been frequently observed in materials since the first discovery in V-Ni-Si and Cr-Ni-Si alloys [54]. Their electron-diffraction patterns reveal that OQCs have multiple length scales [54]. Theoretical studies have pointed out that the formation of OQCs may require correlation potentials with multiple length scales. Concretely, the two-length-scale Landau model, such as the LP model, could obtain a metastable OQC [55], and the four-length-scale model could stabilize OQC [37]. In this section, we apply the SPSM and design a minimal Landau theory to stabilize OQC.

SPSM firstly finds the optimal configuration of primary RLVs of m-length-scale OQC. The length scales and offset angles are

$$q_j=\cos(w_j\pi/8),\quad w_j\in[0,4),\qquad j=1,\ldots,m,$$
$$\theta_1=0,\ \theta_{j'}=s_{j'}\pi/8,\quad s_{j'}\in[0,2),\quad j'=2,\ldots,m.$$

For a specific configuration involving variables $w_1^i,\ldots,w_m^i,s_2^i,\ldots,s_m^i$, the Landau model is written as a polynomial with the minimal value $\mathcal{F}_m^i(*)$. The configuration yielding the lowest $\mathcal{F}_m^i(*)$ is considered optimal. Taking $m=3$ as an example, Fig. 4(a) plots $\mathcal{F}_m^i(*)$ against w_1 and w_2 when fixing $w_3=3$, $s_2=1$, and $s_3=0$. The energy surface is almost flat except for a few peaks. This implies that only a few configurations can significantly lower free energies. The lowest peak whose energy is denoted as $\mathcal{F}_{ref}$ occurs at $(w_1,w_2)=(1,2)$. The corresponding primary RLVs have length scales of $\cos(\pi/8)$, $\cos(\pi/4)$, and $\cos(3\pi/8)$. We have confirmed that this configuration remains optimal as w_3, s_2 and s_3 change. In this optimal configuration, there are two different ways to form the three-RLV interaction. One involves two RLVs with equal wave numbers and another RLV with a different wave number, as illustrated in Fig. 4(b). Another way involves three RLVs with different wave numbers, as shown in Fig. 4(c). The HC free energy of the optimal configuration has the following expression:

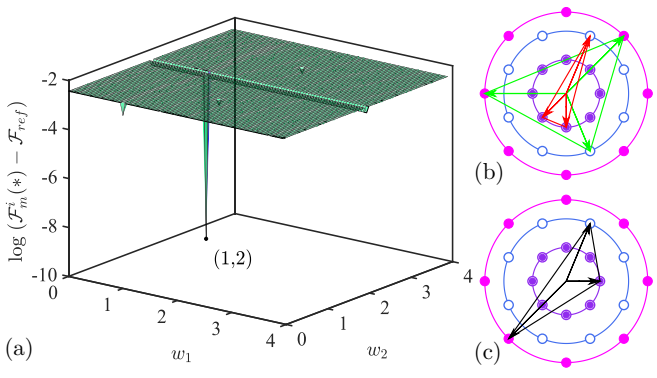

FIG. 4. (a) Free energies of OQC^3 as a function of w_1 and w_2. $w_3=3, s_2=1, s_3=0$. $\mathcal{F}_m^i(*)$ is the minimal value of the HC model with $\epsilon^*=0$. $(w_1,w_2)=(1,2)$ is the peak point with free energy $\mathcal{F}_{ref}=-3.7285\times10^{-3}$. At the peak point, the primary RLVs with length scales $\cos(\pi/8)$, $\cos(\pi/4)$, $\cos(3\pi/8)$ have two types of three-RLV interactions, as shown in (b) and (c).

$$\mathcal{F}_{\mathrm{OQC}^3}\left(\{\hat{\phi}\}_{j=1}^3,\epsilon^*\right) =-4\epsilon^*\sum_{j=1}^3\hat{\phi}_j^2-16\hat{\phi}_2(\hat{\phi}_1+\hat{\phi}_3)^2 +42\sum_{j=1}^3\hat{\phi}_j^4+192\hat{\phi}_1\hat{\phi}_2^2\hat{\phi}_3+48\hat{\phi}_1\hat{\phi}_3\left(\hat{\phi}_1^2+\hat{\phi}_3^2\right) +144\left(\hat{\phi}_1^2\hat{\phi}_2^2+\hat{\phi}_1^2\hat{\phi}_3^2+\hat{\phi}_2^2\hat{\phi}_3^2\right). \tag{16}$$

Moreover, for $m=2$, the optimal primary RLVs of OQC have length scales of 1 and $\cos(\pi/4)$, which are depicted in the embedded pattern of Fig. 5(a), with the HC free energy expressed as

$$\mathcal{F}_{\mathrm{OQC}^2}\left(\{\hat{\phi}\}_{j=1}^2,\epsilon^*\right)=-4\epsilon^*\sum_{j=1}^2\hat{\phi}_j^2-16\hat{\phi}_1\hat{\phi}_2^2 +42\sum_{j=1}^2\hat{\phi}_j^4+120\hat{\phi}_1^2\hat{\phi}_2^2. \tag{17}$$

To study the thermodynamic stability of OQCs under HC, Fig. 5(a) plots the HC free energy of candidate structures as a function of ϵ^* for a Landau model with two length scales 1 and $\cos(\pi/4)$. We find that SQU^2 is favorable when $\epsilon^*\leqslant0.7688$, HEX^1 for $0.7688\leqslant\epsilon^*\leqslant1.9159$, and LAM^1 when $\epsilon^*\gtrsim1.9159$. Thus the two-length-scale OQC is metastable. For a Landau model with three length scales $\cos(\pi/8)$, $\cos(\pi/4)$, and $\cos(3\pi/8)$, we find stable OQCs when $\epsilon^*\leqslant0.0300$, as shown in Fig. 5(b). The reason could be attributed that the primary RLVs in the three-length-scale OQC form more three-RLV interactions than those in the two-length-scale OQC, thereby reducing the HC free energy. Furthermore, the HC phase diagram in the ϵ-α plane is plotted in Fig. 5(c). Here, the three-length-scale OQC is expected to be thermodynamic stable when $-0.1021\leqslant\epsilon^*\leqslant0.0300$. Therefore, this three-length-scale Landau model is the minimal model to stabilize OQC under HC.

Based on the HC minimal Landau model, we further study the thermodynamic stability of OQC under SC to design a SC minimal Landau theory. We apply the projection method to evaluate OQCs and their free energies accurately. Fig. 6(a_1) depicts the coordinates of the optimal primary RLVs of OQCs in two-dimensional space. To be consistent with the rescaling model (10), the length scales are measured in units of q_3. We set the four vectors (1,0), $(\sqrt{2}/2,\sqrt{2}/2)$, (0,1), $(-\sqrt{2}/2,\sqrt{2}/2)$ as basis vectors, allowing the primary RLVs to be expressed by integer coefficients with the four vectors, as illustrated in Fig. 6(a_2). Accordingly, the projection matrix is

$$\mathcal{P}_{OQC}=\begin{pmatrix}1&\sqrt{2}/2&0&-\sqrt{2}/2\\0&\sqrt{2}/2&1&\sqrt{2}/2\end{pmatrix}. \tag{18}$$

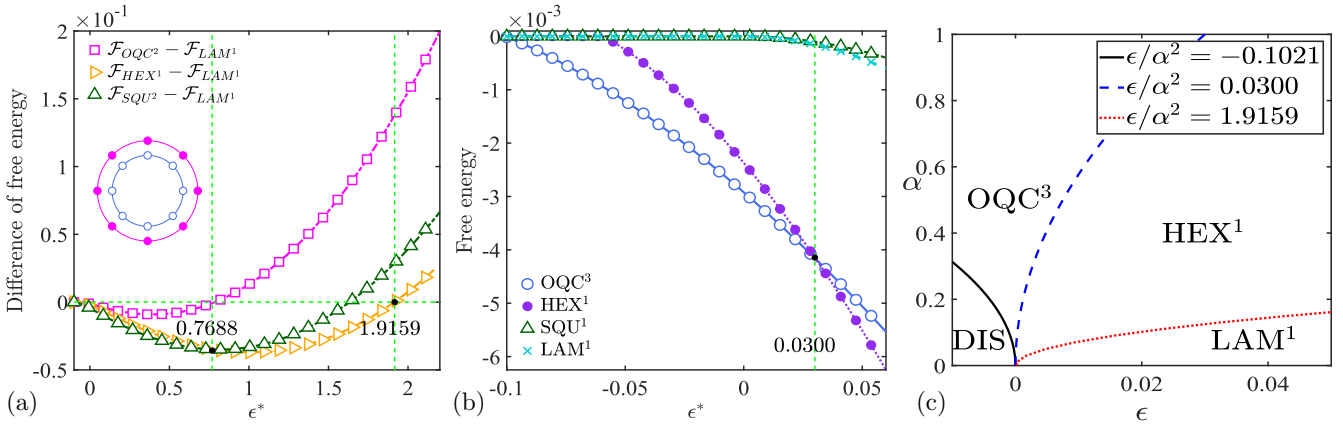

FIG. 5. (a) HC free energy of two-length-scale candidate phases with the energy of LAM^1 as the baseline. Two length scales are 1 and $\cos(\pi/4)$. The embedded pattern is the optimal primary RLVs of OQC^2. (b) Free energies of candidate structures in the HC model with three length scales $\cos(\pi/8)$, $\cos(\pi/4)$, and $\cos(3\pi/8)$. (c) HC phase diagram of the three-length-scale model in ϵ-α plane. DIS stands for the disordered phase with zero free energy.

The OQC is embedded into a four-dimensional periodic structure that can be accurately calculated, and then it is recovered by projecting this four-dimensional periodic structure into the two-dimensional space.

In Figs. 6(a)–6(d), we present the diffraction patterns and real-space morphologies of stationary candidate structures. Figure 6(e) plots the Fourier transform of correlation potential whose roots correspond to the three length scales. Figure 6(f) presents the SC phase diagram, where OQC^3, HEX^1, and LAM^1 occupy stable regions but SQU^1 remains metastable. The phase boundaries in the SC phase diagram are similar to those in the HC phase diagram Fig. 5(c). It may be attributed to the fact that the primary RLVs play a dominant role in determining the stability of candidate structures and the contribution of nonprimary RLVs causes slight changes in phase boundaries. Consequently, we could come to a conclusion that the minimal Landau theory to stabilize OQCs under SC involves three length scales $\cos(\pi/8)$, $\cos(\pi/4)$, and $\cos(3\pi/8)$.

In previous study on primary RLVs of OQCs, only a finite number of configurations were considered [37,55]. SPSM examines nearly all possible configurations and effectively

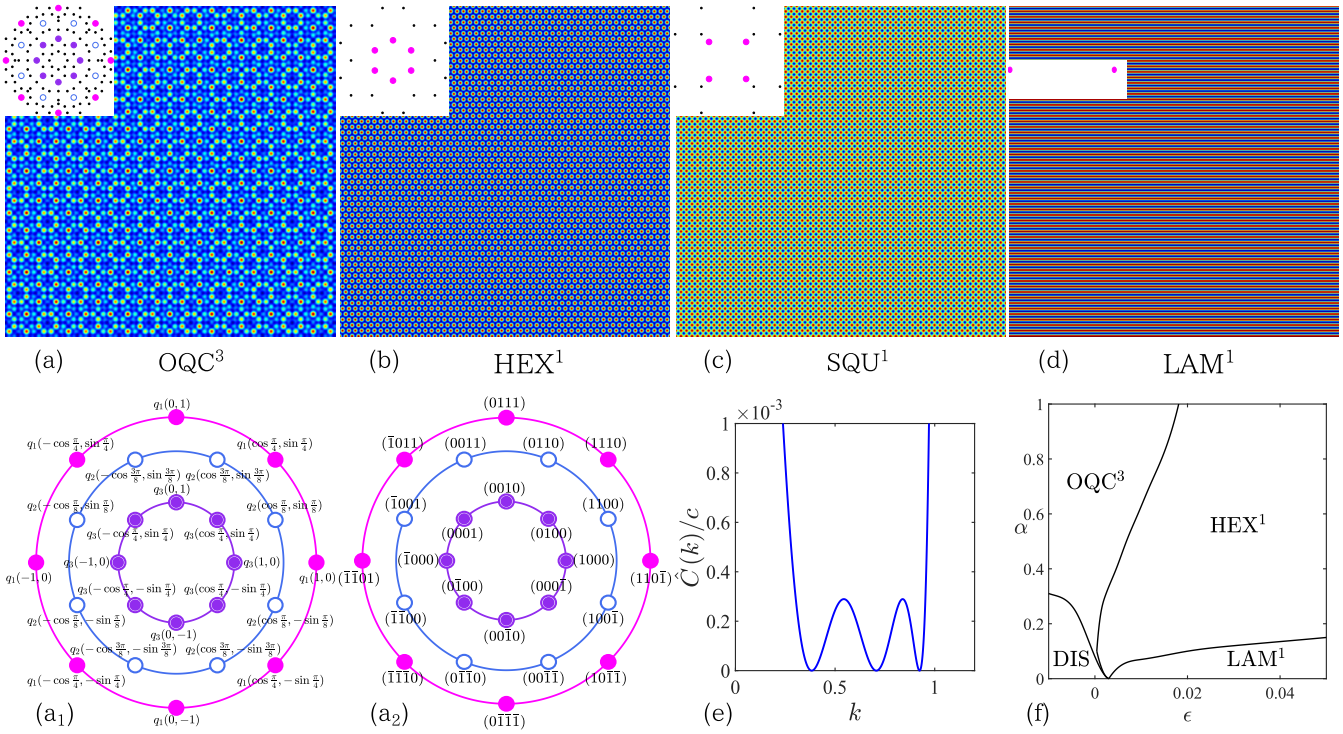

FIG. 6. Coordinates of optimal primary RLVs of OQC^3 in (a$_1$) two-dimensional and (a$_2$) four-dimensional reciprocal space. Stationary ordered states: (a) OQC^3; (b) HEX^1; (c) SQU^1; (d) LAM^1 calculated by the projection method in the Landau model with three length scales $\cos(\pi/8)$, $\cos(\pi/4)$, and $\cos(3\pi/8)$. The diffraction pattern embedded in the upper left corner only plots these RLVs with intensities greater than 10^{-6}. (e) Fourier transform of correlation potential in units of c. (f) SC phase diagram of the three-length-scale model.

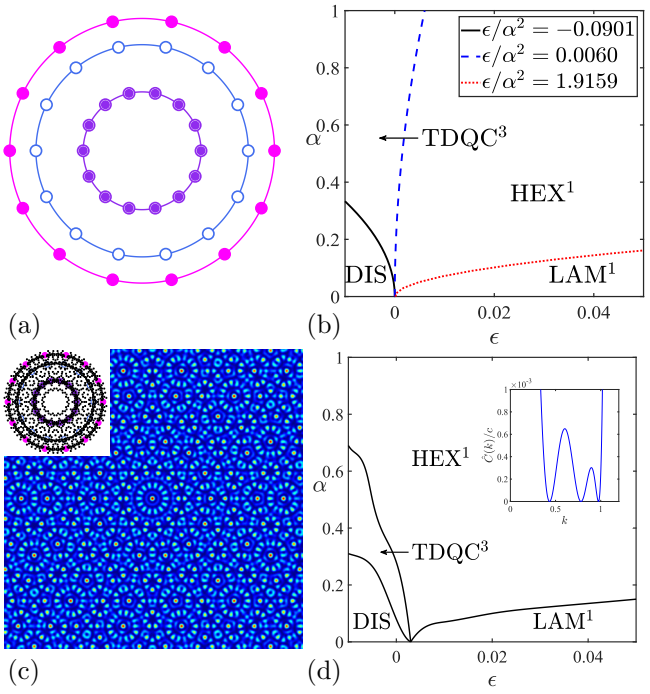

FIG. 7. (a) Optimal primary RLVs of TDQC^3, (b) HC phase diagram, (c) stationary patterns of TDQC^3 at $\epsilon = -0.01$ and $\alpha = 0.5$, and (d) SC phase diagram and correlation potential. The three length scales are $\cos(\pi/14)$, $\cos(3\pi/14)$, and $\cos(5\pi/14)$.

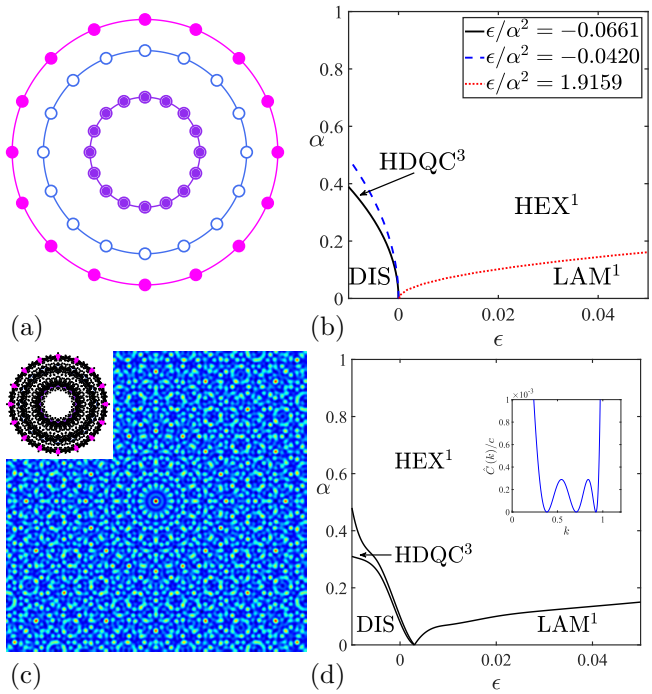

FIG. 8. (a) Optimal primary RLVs of HDQC^3, (b) HC phase diagram, (c) stationary patterns at $\epsilon = -0.01$ and $\alpha = 0.4$, and (d) SC phase diagram and correlation potential. The three length scales are $\cos(\pi/8)$, $\cos(\pi/4)$, and $\cos(3\pi/8)$.

identifies the optimal configuration. Therefore, SPSM can design a minimal Landau theory to stabilize OQCs.

B. Tetradecagonal (TD), hexadecagonal (HD), and octadecagonal (OD) QCs

To the best of our knowledge, TDQC and HDQC have not yet been observed in nature and laboratories. Utilizing SPSM, we design minimal Landau theories to stabilize these structures, which may be helpful for experimental research. Numerical results demonstrate that the minimal Landau theories both have three length scales.

For the three-length-scale TDQC, we present its optimal configuration of primary RLVs in Fig. 7(a). The corresponding HC free energy is

$$\begin{aligned}\mathcal{F}_{\mathrm{TDQC}^3}&\left(\{\hat{\phi}\}_{j=1}^4, \epsilon^*\right)\\ &= -7\epsilon^*\sum_{j=1}^3\hat{\phi}_j^2 - 56\hat{\phi}_1\hat{\phi}_2\hat{\phi}_3\\ &\quad - 28\left(\hat{\phi}_1^2\hat{\phi}_3 + \hat{\phi}_1\hat{\phi}_2^2 + \hat{\phi}_2\hat{\phi}_3^2\right) + \frac{273}{2}\sum_{j=1}^3\hat{\phi}_j^4\\ &\quad + 252\hat{\phi}_1\hat{\phi}_2\hat{\phi}_3\sum_{j=1}^3\hat{\phi}_j + 84\left(\hat{\phi}_1^3\hat{\phi}_2 + \hat{\phi}_1\hat{\phi}_3^3 + \hat{\phi}_2^3\hat{\phi}_3\right)\\ &\quad + 378\left(\hat{\phi}_1^2\hat{\phi}_2^2 + \hat{\phi}_1^2\hat{\phi}_3^2 + \hat{\phi}_2^2\hat{\phi}_3^2\right). \qquad (19)\end{aligned}$$

Figure 7(b) plots the HC phase diagram, where TDQC^3 is stable when $-0.0901 \leqslant \epsilon^* \leqslant 0.0060$. Under SC, Fig. 7(c) displays the stationary patterns of TDQC^3 computed by the projection method. More details on the projection matrix and high-dimensional coordinates can be found in Eq. (S4) and Fig. S1(d), respectively, within the SM [53]. Figure 7(d) shows the SC phase diagram, revealing a stable region for TDQC^3. The embedded pattern represents the Fourier transform of correlation potential.

For the three-length-scale HDQC, Fig. 8(a) presents the optimal configuration of primary RLVs, which results in the HC free energy

$$\begin{aligned}\mathcal{F}_{\mathrm{HDQC}^3}&\left(\{\hat{\phi}\}_{j=1}^4, \epsilon^*\right)\\ &= -8\epsilon^*\sum_{j=1}^3\hat{\phi}_j^2 - 32\hat{\phi}_2(\hat{\phi}_1 + \hat{\phi}_3)^2\\ &\quad + 180\sum_{j=1}^3\hat{\phi}_j^4 + 96\hat{\phi}_1\hat{\phi}_3\left(\hat{\phi}_1^2 + \hat{\phi}_3^2\right) + 384\hat{\phi}_1\hat{\phi}_2^2\hat{\phi}_3\\ &\quad + 480\left(\hat{\phi}_1^2\hat{\phi}_2^2 + \hat{\phi}_1^2\hat{\phi}_3^2 + \hat{\phi}_2^2\hat{\phi}_3^2\right). \qquad (20)\end{aligned}$$

We plot the corresponding HC phase diagram in Fig. 8(b), indicating that HDQC^3 is thermodynamic stable for $-0.0661 \leqslant \epsilon^* \leqslant -0.0420$. Under SC, we use the projection method and obtain the stationary pattern of HDQC^3 as shown in Fig. 8(c). We give the projection matrix in Eq. (S5) and high-dimensional coordinates of HDQC^3 in Fig. S1(e) within the SM [53]. Figure 8(d) plots the SC phase diagram, confirming the stability of HDQC^3 under SC, and shows the pattern of correlation potential in Fourier space.

ODQC has been discovered in soft colloidal systems, as evidenced by their diffraction patterns that exhibit multiple

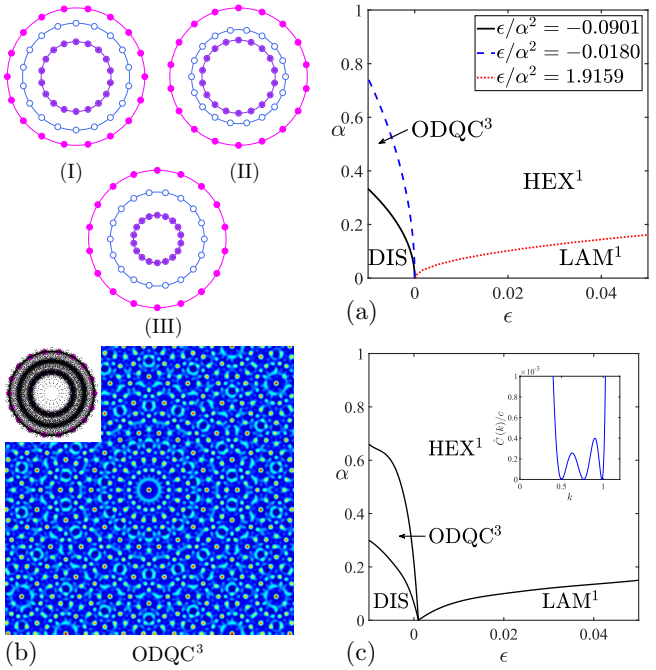

FIG. 9. Optimal primary RLVs of ODQC^3 whose radii of the circles from outside to inside are (I) $\cos(\pi/18)$, $\cos(2\pi/9)$, $1/2$; (II) $\cos(\pi/9)$, $\cos(5\pi/18)$, $1/2$; (III) $1/2$, $\cos(7\pi/18)$, $\cos(4\pi/9)$. (a) HC phase diagram of the three-length-scale model in ϵ-α plane. (b) Stationary patterns of ODQC^3 at $\epsilon = -0.01$ and $\alpha = 0.5$. Nonprimary RLVs with intensities greater than 10^{-6} are indicated by small dots. (c) Phase diagram of the SC minimal Landau model with three length scales $\cos(\pi/18)$, $\cos(2\pi/9)$, and $1/2$. The pattern of $\hat{C}(k)$ is embedded in (c).

length scales [17]. Stable ODQCs in theoretical study have been obtained by a Landau model with four length scales [37]. In our study, we design three minimal Landau models by SPSM, each with three different length scales: (I) $\cos(\pi/18)$, $\cos(2\pi/9)$, $1/2$; (II) $\cos(\pi/9)$, $\cos(5\pi/18)$, $1/2$; (III) $1/2$, $\cos(7\pi/18)$, $\cos(4\pi/9)$. Figures 9(I)–9(III) show the optimal configurations of primary RLVs of ODQCs, corresponding to the minimal models (I)–(III) respectively. These configurations have the same number of three- and four-RLV interactions, resulting in the same HC free energy

$$\begin{aligned}\mathcal{F}_{\mathrm{ODQC}^3}&\left(\{\hat{\phi}\}_{j=1}^3, \epsilon^*\right)\\ &= -9\epsilon^*\sum_{j=1}^3\hat{\phi}_j^2 - 12\sum_{j=1}^3\hat{\phi}_j^3\\ &\quad - 36\hat{\phi}_1\sum_{j=2}^3\hat{\phi}_j^2 - 36\hat{\phi}_2\hat{\phi}_3(2\hat{\phi}_1+\hat{\phi}_3) + \frac{459}{2}\sum_{j=1}^3\hat{\phi}_j^4\\ &\quad + 108\hat{\phi}_2^3(2\hat{\phi}_1+\hat{\phi}_3) + 216\hat{\phi}_3^3(\hat{\phi}_1+\hat{\phi}_2) + 702\hat{\phi}_2^2\hat{\phi}_3^2\\ &\quad + 702\hat{\phi}_1^2\left(\hat{\phi}_2^2+\hat{\phi}_3^2\right) + 756\hat{\phi}_1^2\hat{\phi}_2\hat{\phi}_3\\ &\quad + 432\hat{\phi}_1\hat{\phi}_2\hat{\phi}_3(\hat{\phi}_2+\hat{\phi}_3). \end{aligned} \tag{21}$$

Figure 9(a) plots the HC phase diagram, where ODQC^3 is expected to be thermodynamic stable in $-0.0901 \leqslant \epsilon^* \leqslant -0.0180$. Moreover, we take the minimal model (I) as an example to examine the thermodynamic stability of ODQCs under SC. The embedded pattern of Fig. 9(c) depicts the Fourier transform of correlation potential about the three length scales. By use of the projection method [see Eq. (S6) for projection matrix and Fig. S1(f) for high-dimensional coordinates within the SM [53]], we obtain the stationary ODQC^3 phase. Its diffraction pattern and real-space morphology are shown in Fig. 9(b). Figure 9(c) presents the SC phase diagram, revealing a stable region for ODQC^3. The phase boundaries exhibit a slight shift compared to the HC phase diagram, which may be attributed to the nonnegligible influence of nonprimary RLVs and the predominant contribution of primary RLVs. Moreover, we find stable ODQC^3 in the models (II) and (III) with SC.

IV. CONCLUSIONS

In this paper, we propose an efficient method (SPSM) to design a minimal Landau theory to stabilize desired QCs. SPSM evaluates almost all possible configurations of RLVs for the target QC, allowing us to identify the optimal configuration with the lowest free energy, as the free-energy functional can be expressed as a polynomial under HC. With this optimal configuration, SPSM then constructs phase diagrams to assess the thermodynamic stability of the target QC. Generally, configurations with more length scales contain more primary RLVs, which can form more three-RLV interactions to lower the free energy. Thus, we can always design a minimal Landau theory to stabilize desired QCs by gradually increasing the number of length scales.

Using SPSM, we design minimal Landau theories to stabilize $2n$-fold QCs ($n = 4, \ldots, 9$). Concretely, two-length-scale Landau models can stabilize 10- and 12-fold QCs, which is consistent with previous results. Moreover, we obtain stable 8- and 18-fold QCs in three-length-scale Landau models, reducing the number of length scales compared to earlier studies. Our findings also indicate that three-length-scale models can stabilize 14- and 16-fold QCs. We believe that these minimal models with relatively simple potentials could be helpful to control the synthesis of QCs.

ACKNOWLEDGMENTS

The work is supported in part by the National Key R&D Program of China (Grant No. 2023YFA1008802), the National Natural Science Foundation of China (Grants No. 12171412, and No. 12288101), the Science and Technology Innovation Program of Hunan Province (Grant No. 2024RC1052), the Innovative Research Group Project of Natural Science Foundation of Hunan Province of China (Grant No. 2024JJ1008), the China Postdoctoral Science Foundation (Grant No. 2024T170674), and the Natural Sciences and Engineering Research Council of Canada. We are also grateful to the High Performance Computing Platform of Xiangtan University for partial support of this work.

There are no conflicts to declare.

DATA AVAILABILITY

The data supporting this study's findings are available within the article.

[1] D. Shechtman, I. Blech, D. Gratias, and J. W. Cahn, Metallic phase with long-range orientational order and no translational symmetry, Phys. Rev. Lett. **53**, 1951 (1984).

[2] W. Steurer, Twenty years of structure research on quasicrystals. Part I. Pentagonal, octagonal, decagonal and dodecagonal quasicrystals, Z. Kristallogr. **219**, 391 (2004).

[3] X. Zeng, G. Ungar, Y. Liu, V. Percec, A. E. Dulcey, and J. K. Hobbs, Supramolecular dendritic liquid quasicrystals, Nature (London) **428**, 157 (2004).

[4] C. Duan, M. Zhao, Y. Qiang, L. Chen, W. Li, F. Qiu, and A.-C. Shi, Stability of two-dimensional dodecagonal quasicrystalline phase of block copolymers, Macromolecules **51**, 7713 (2018).

[5] A. J. Archer, T. Dotera, and A. M. Rucklidge, Rectangle-triangle soft-matter quasicrystals with hexagonal symmetry, Phys. Rev. E **106**, 044602 (2022).

[6] Y. Liu, T. Liu, X.-Y. Yan, Q.-Y. Guo, H. Lei, Z. Huang, R. Zhang, Y. Wang, J. Wang, F. Liu *et al.*, Expanding quasiperiodicity in soft matter: Supramolecular decagonal quasicrystals by binary giant molecule blends, Proc. Natl. Acad. Sci. USA **119**, e2115304119 (2022).

[7] M. Suzuki, T. Orido, A. Takano, and Y. Matsushita, The largest quasicrystalline tiling with dodecagonal symmetry from a single pentablock quarterpolymer of the AB_1CB_2D type, ACS Nano **16**, 6111 (2022).

[8] X. Zeng, B. Glettner, U. Baumeister, B. Chen, G. Ungar, F. Liu, and C. Tschierske, A columnar liquid quasicrystal with a honeycomb structure that consists of triangular, square and trapezoidal cells, Nat. Chem. **15**, 625 (2023).

[9] E. Fayen, M. Impéror-Clerc, L. Filion, G. Foffi, and F. Smallenburg, Self-assembly of dodecagonal and octagonal quasicrystals in hard spheres on a plane, Soft Matter **19**, 2654 (2023).

[10] H. Löwen, Melting, freezing and colloidal suspensions, Phys. Rep. **237**, 249 (1994).

[11] V. Percec, M. R. Imam, M. Peterca, D. A. Wilson, R. Graf, H. W. Spiess, V. S. Balagurusamy, and P. A. Heiney, Self-assembly of dendronized triphenylenes into helical pyramidal columns and chiral spheres, J. Am. Chem. Soc. **131**, 7662 (2009).

[12] Y. Cao, A. Scholte, M. Prehm, C. Anders, C. Chen, J. Song, L. Zhang, G. He, C. Tschierske, and F. Liu, Understanding the role of trapezoids in honeycomb self-assembly—Pathways between a columnar liquid quasicrystal and its liquid-crystalline approximants, Angew. Chem. Int. Ed. **63**, e202314454 (2024).

[13] K. Hayashida, T. Dotera, A. Takan, and Y. Matsushita, Polymeric quasicrystal: Mesoscopic quasicrystalline tiling in ABC star polymers, Phys. Rev. Lett. **98**, 195502 (2007).

[14] Y. Mai and A. Eisenberg, Self-assembly of block copolymers, Chem. Soc. Rev. **41**, 5969 (2012).

[15] J. Zhang and F. S. Bates, Dodecagonal quasicrystalline morphology in a poly (styrene-b-isoprene-b-styrene-b-ethylene oxide) tetrablock terpolymer, J. Am. Chem. Soc. **134**, 7636 (2012).

[16] Q. Xie, Y. Qiang, and W. Li, Regulate the stability of gyroids of ABC-type multiblock copolymers by controlling the packing frustration, ACS Macro Lett. **9**, 278 (2020).

[17] S. Fischer, A. Exner, K. Zielske, J. Petrich, S. Deloudi, W. Steurer, P. lindner, and S. Företer, Colloidal quasicrystals with 12-fold and 18-fold diffraction symmetry, Proc. Natl. Acad. Sci. USA **108**, 1810 (2011).

[18] C. G. Sztrum and E. Rabani, Out-of-equilibrium self-assembly of binary mixtures of nanoparticles, Adv. Mater. **18**, 565 (2006).

[19] D. V. Talapin, E. V. Shevchenko, M. I. Bodnarchuk, X. Ye, J. Chen, and C. B. Murray, Quasicrystalline order in self-assembled binary nanoparticle superlattices, Nature (London) **461**, 964 (2009).

[20] T. Dotera and T. Gemma, Dodecagonal quasicrystal in a polymeric alloy, Philos. Mag. **86**, 1085 (2006).

[21] Y. Miyamori, J. Suzuki, A. Takano, and Y. Matsushita, Periodic and aperiodic tiling patterns from a tetrablock terpolymer system of the A_1BA_2C type, ACS Macro Lett. **9**, 32 (2020).

[22] A. P. Lindsay III, R. M. 3rd Lewis, B. Lee, A. J. Peterson, T. P. Lodge, and F. S. Bates, A15, σ and a quasicrystal: Access to complex particle packings via bidisperse diblock copolymer blends, ACS Macro Lett. **9**, 197 (2020).

[23] A. P. Tsai, Icosahedral clusters, icosahedral order and stability of quasicrystals—A view of metallurgy, Sci. Technol. Adv. Mater. **9**, 013008 (2008).

[24] M. N. van der Linden, J. P. K. Doye, and A. A. Louis, Formation of dodecagonal quasicrystals in two-dimensional systems of patchy particles, J. Chem. Phys. **136**, 054904 (2012).

[25] T. Dotera, Mean-field theory of Archimedean and quasicrystalline tilings, Philos. Mag. **87**, 3011 (2007).

[26] R. Lifshitz and H. Diamant, Soft quasicrystals—Why are they stable? Philos. Mag. **87**, 3021 (2007).

[27] K. Barkan, H. Diamant, and R. Lifshitz, Stability of quasicrystals composed of soft isotropic particles, Phys. Rev. B **83**, 172201 (2011).

[28] J. Yin, K. Jiang, A.-C. Shi, P. Zhang, and L. Zhang, Transition pathways connecting crystals and quasicrystals, Proc. Natl. Acad. Sci. USA **118**, e2106230118 (2021).

[29] G. Cui, K. Jiang, and T. Zhou, An efficient saddle search method for ordered phase transitions involving translational invariance, Comput. Phys. Commun. **306**, 109381 (2025).

[30] J. P. Hansen and I. R. McDonald, *Theory of Simple Liquids*, 4th ed. (Elsevier Academic Press, Amsterdam, 2013).

[31] C. N. Likos, Effective interactions in soft condensed matter physics, Phys. Rep. **348**, 267 (2001).

[32] S. A. Brazovskii, Phase transition of an isotropic system to a nonuniform state, Sov. Phys.-JETP **41**, 85 (1975).

[33] J. Swift and P. C. Hohenberg, Hydrodynamic fluctuations at the convective instability, Phys. Rev. A **15**, 319 (1977).

[34] R. Lifshitz and D. M. Petrich, Theoretical model for faraday waves with multiple-frequency forcing, Phys. Rev. Lett. **79**, 1261 (1997).

[35] B. Echebarria, R. Folch, A. Karma, and M. Plapp, Quantitative phase-field model of alloy solidification, Phys. Rev. E **70**, 061604 (2004).

[36] K. Jiang, P. Zhang, and A.-C. Shi, Stability of icosahedral quasicrystals in a simple model with two-length scales, J. Phys.: Condens. Matter **29**, 124003 (2017).

[37] S. Savitz, M. Babadi, and R. Lifshitz, Multiple-scale structures: From Faraday waves to soft-matter quasicrystals, IUCrJ. **5**, 247 (2018).

[38] K. Jiang and W. Si, Stability of three-dimensional icosahedral quasicrystals in multi-component systems, Philos. Mag. **100**, 84 (2020).

[39] A. J. Archer, A. M. Rucklidge, and E. Knobloch, Quasicrystalline order and a crystal-liquid state in a soft-core fluid, Phys. Rev. Lett. **111**, 165501 (2013).

[40] T. Dotera, T. Oshiro, and P. Ziherl, Mosaic two-lengthscale quasicrystals, Nature (London) **506**, 208 (2014).

[41] K. Barkan, M. Engel, and R. Lifshitz, Controlled self-assembly of periodic and aperiodic cluster crystals, Phys. Rev. Lett. **113**, 098304 (2014).

[42] P. Subramanian, A. J. Archer, E. Knobloch, and A. M. Rucklidge, Three-dimensional icosahedral phase field quasicrystal, Phys. Rev. Lett. **117**, 075501 (2016).

[43] C. Liang, K. Jiang, S. Tang, J. Wang, Y. Ma, W. Liu, and Y. Du, Molecular-level insights into the nucleation mechanism of one-component soft matter icosahedral quasicrystal studied by phase-field crystal simulations, Cryst. Growth Des. **22**, 2637 (2022).

[44] C. Reich, M. Conrad, F. Krumeich, and B. Harbrecht, The dodecagonal quasicrystalline telluride $(\mathrm{Ta},\ \mathrm{V})_{1.6}\mathrm{Te}$ and its crystalline approximant $(\mathrm{TaV})_{97}\mathrm{Te}_{60}$, MRS Proc. **553**, 83 (1998).

[45] S. K. Mkhonta, K. R. Elder, and Z.-F. Huang, Exploring the complex world of two-dimensional ordering with three modes, Phys. Rev. Lett. **111**, 035501 (2013).

[46] D. J. Ratliff, A. J. Archer, P. Subramanian, and A. M. Rucklidge, Which wave numbers determine the thermodynamic stability of soft matter quasicrystals? Phys. Rev. Lett. **123**, 148004 (2019).

[47] K. Jiang and P. Zhang, Numerical methods for quasicrystals, J. Comput. Phys. **256**, 428 (2014).

[48] K. Jiang, S. Li, and P. Zhang, Numerical methods and analysis of computing quasiperiodic systems, SIAM J. Numer. Anal. **62**, 353 (2024).

[49] K. Jiang, W. Si, C. Chen, and C. Bao, Efficient numerical methods for computing the stationary states of phase field crystal models, SIAM J. Sci. Comput. **42**, B1350 (2020).

[50] C. Bao, C. Chen, and K. Jiang, An adaptive block Bregman proximal gradient method for computing stationary states of multicomponent phase-field crystal model, CSIAM Trans. Appl. Math. **3**, 133 (2022).

[51] C. Bao, C. Chen, K. Jiang, and L. Qiu, Convergence analysis for Bregman iterations in minimizing a class of Landau free energy functionals, SIAM J. Numer. Anal. **62**, 476 (2024).

[52] K. Jiang and W. Si, Automatically generating phase diagram (AGPD) 1.0, Software copyright registration certificate, National Copyright Administration of the People's Republic of China: 2022SR0139033 (2022), https://github.com/KaiJiangMath/AGPD.

[53] See Supplemental Material at http://link.aps.org/supplemental/10.1103/PhysRevResearch.7.023021 for the numerical results of $2n$-fold quasicrystals with two, three and four length scales ($n = 4, \ldots, 9$). The results include the optimal primary RLVs, the formula of HC free energies, HC phase diagrams, the projection matrix, high-dimensional coordinates, the stationary patterns, and SC phase diagrams.

[54] N. Wang, H. Chen, and K. H. Kuo, Two-dimensional quasicrystal with eightfold rotational symmetry, Phys. Rev. Lett. **59**, 1010 (1987).

[55] K. Jiang, J. Tong, P. Zhang, and A.-C. Shi, Stability of two-dimensional soft quasicrystals, Phys. Rev. E **92**, 042159 (2015).